Meshless Multi-Point Flux Approximation

Alexander A. Lukyanov and Cornelis Vuik

Abstract The reservoir simulation of the complex reservoirs with anisotropic permeability, which includes faults and non-orthogonal grids, with a fully discontinuous permeability tensor in the discretization is a major challenge. Several methods have already been developed and implemented within industry standard reservoir simulators for non-orthogonal grids (e.g., Multi-Point Flux Approximation (MPFA) "O" method). However, it has been noticed that some of the numerical methods for elliptic/parabolic equations may violate the maximum principle (i.e., lead to spurious oscillations), especially when the anisotropy is particularly strong. It has been found that the oscillations are closely related to the poor approximation of the pressure gradient in the flux computation. Therefore, proposed methods must correctly approximate underlying operators, satisfy a discrete maximum principle and have coercivity properties. Furthermore, the method must be robust and efficient. This paper presents the meshless multi-point flux approximation of second order elliptic operators containing a tensor coefficient. The method is based on a pressure gradient approximation commonly used in meshless methods (or Smoothed Particle Hydrodynamics method—SPH method). The proposed discretization schemes can be written as a sum of sparse positive semidefinite matrix and perturbation matrix. We show that convergence rates are retained as for finite difference methods $O(h^{\alpha}),\ 1 \leq \alpha < 2$, where h denotes the maximum particle spacing. The results are presented, discussed and future studies are outlined.

A.A. Lukyanov (✉)
Schlumberger-Doll Research, One Hampshire Street, Cambridge, MA 02139, USA
e-mail: alukyanov@slb.com

C. Vuik
Faculty of Electrical Engineering, Mathematics and Computer Science (EEMCS), Delft Institute of Applied Mathematics, Delft University of Technology, 2628 CD Delft, The Netherlands
e-mail: c.vuik@tudelft.nl

M. Griebel, M.A. Schweitzer (eds.), *Meshfree Methods for Partial Differential Equations VIII*, Lecture Notes in Computational Science and Engineering 115,
DOI 10.1007/978-3-319-51954-8_5

1 Introduction

The multi-point flux approximation, MPFA, is a discretization method developed by the oil industry to be the next generation method in reservoir simulations and it can be applied to different types of mesh, for example using quadrilateral meshes as in Aavatsmark et al. [2, 3], Aavatsmark [1], Edwards and Rogers [12], Klausen and Russell [17] or unstructured grids as in Edwards [11] to approximate the following operator:

$$\mathbf{L}\left(p\left(\mathbf{r}\right)\right) = -\nabla\left(\mathbf{M}\left(\mathbf{r}, p\left(\mathbf{r}\right)\right)\nabla p\left(\mathbf{r}\right)\right) - g\left(\mathbf{r}\right), \ \forall \mathbf{r} \in \Omega \subset \mathbb{R}^n \tag{1}$$

where $p\left(\mathbf{r}\right)$ is the pressure, $\mathbf{M}\left(\mathbf{r}, p\left(\mathbf{r}\right)\right) = \left(m_{\alpha\beta}\right)$ is the mobility tensor, $g\left(\mathbf{r}\right)$ is the known sink / source term, $n = 1, 2, 3$ is the spatial dimension. Consider the operator in the expression (1) with a piecewise constant mobility $\mathbf{M}\left(\mathbf{r}, p\left(\mathbf{r}\right)\right) \in L_2\left(\Omega\right)$.

Several methods have already been developed and implemented within an industry standard reservoir simulator for non-orthogonal grids. The methods are known as the O-method, U-method and the L-method for quadrilateral meshes in two and three dimensions (see [1, 12, 18]. The MPFA methods are not restricted to quadrilateral meshes and have been investigated in Edwards [11]. It has been noticed that some of the numerical methods for elliptic/parabolic equations may violate the maximum principle (i.e. lead to spurious oscillations). Therefore, proposed methods must satisfy a discrete maximum principle to avoid any spurious oscillations. The discrete maximum principle for MPFA methods was discussed, e.g., in Edwards and Rogers [12], Mlacnik and Durlofsky [28], Lee et al. [19].

However, non-physical oscillations can appear in the developed multi-point flux approximations when the anisotropy is particularly strong. It has been found that the oscillations are closely related to the poor approximation of the pressure gradient in the flux computation. In this paper, the meshless multi-point flux approximation for the general fluid flow in porous media is proposed. The discretization scheme is based both on the generalized Laplace approximation and on a gradient approximation commonly used in the Smoothed Particle Hydrodynamics (SPH) community for thermal, viscous, and pressure projection problems and can be extended to include higher-order terms in the appropriate Taylor series. The proposed discretization scheme is combined with mixed corrections, which ensure linear completeness. The mixed correction utilizes Shepard Functions in combination with a correction to derivative approximations. Incompleteness of the kernel support combined with the lack of consistency of the kernel interpolation in conventional meshless methods results in fuzzy boundaries. In corrected meshless methods, the domain boundaries and field variables at the boundaries are approximated with the improved accuracy comparing to the conventional SPH method. The resulting schemes improve the particle deficiency (kernel support incompleteness) problem. Although, the analysis of the different discretization schemes in this paper is restricted to 2D (i.e., $n = 2$), the results can be applied in any space.

2 Fluid Flow Modelling Using SPH

To calculate the second derivatives of $\mathbf{F}$, several methods were proposed (Chen et al. [7]; Bonet and Kulasegaram [4]; Colin et al. [9]). However, second-order derivatives can often be avoided entirely if the PDE is written in a weak form. It is important to note that approximations using second-order derivatives of the kernel are often noisy and sensitive to the particle distributions, particularly for spline kernels of lower orders.

Brookshaw [6] proposed an approximation of the Laplacian for an inhomogeneous scalar field $m(\mathbf{r})$ that only includes first order derivatives:

$$\begin{aligned}&\langle \nabla (m(\mathbf{r}_I) \nabla \mathbf{F}(\mathbf{r}_I))\rangle = \\ &= \sum_{\Omega_{\mathbf{r}_I,h}} V_{\mathbf{r}_J} [\mathbf{F}(\mathbf{r}_J) - \mathbf{F}(\mathbf{r}_I)] \frac{(\mathbf{r}_J - \mathbf{r}_I)\cdot(m_J + m_I)\nabla W(\mathbf{r}_J - \mathbf{r}_I, h)}{\|\mathbf{r}_J - \mathbf{r}_I\|^2}\end{aligned} \tag{2}$$

where $V_{\mathbf{r}_J}$ is the volume of a particle J, $\|\bullet\|$ is the Euclidean norm throughout this paper, $\mathbf{F}(\mathbf{r})$ is the unknown scalar or vector field (e.g., pressure p) $\forall \mathbf{r} \in \Omega \subset \mathbb{R}^n$, $m_I = m(\mathbf{r}_I)$, $\mathbf{r}_I \in \Omega \subset \mathbb{R}^n$ and $m_J = m(\mathbf{r}_J)$, $\mathbf{r}_J \in \Omega \subset \mathbb{R}^n$ are the field coefficients, $W(\mathbf{r}_J - \mathbf{r}_I, h)$ is the Kernel.

This Laplacian approximation was used by Brookshaw [6], Cleary and Monaghan [8], Jubelgas et al. [16] for thermal conduction, Morris et al. [29] for modelling viscous diffusion, Cummins and Rudman [10] for a vortex spin-down and Rayleigh-Taylor instability, Shao and Lo [33] for simulating Newtonian and non-Newtonian flows with a free surface, Moulinec et al. [20] for comparisons of weakly compressible and truly incompressible algorithms, Hu and Adams [15] for macroscopic and mesoscopic flows, Zhang et al. [34] for simulations of the solid-fluid mixture flow. There are several numerical SPH schemes commonly used in numerical simulations for a scalar inhomogeneous field $m(\mathbf{r})$. High order accuracy approximations can also be derived by using SPH discretization based on higher order Taylor series expansions [13, 14, 22, 31]. However, it is usually required that the discrete numerical schemes can reproduce linear fields [5, 23, 27, 30] or polynomials up to a given order [21].

The correction terms to Brookshaw's formulation, which improve the accuracy of the Laplacian operator near boundaries, were proposed by Schwaiger [31]:

$$\begin{aligned}&\langle \nabla (m(\mathbf{r}_I) \nabla \mathbf{F}(\mathbf{r}_I))\rangle = \\ &\frac{\Gamma^{-1}_{\beta\beta}}{n}\left\{\sum_{\Omega_{\mathbf{r}_I,h}} V_{\mathbf{r}_J} [\mathbf{F}(\mathbf{r}_J) - \mathbf{F}(\mathbf{r}_I)] \frac{(\mathbf{r}_J - \mathbf{r}_I)\cdot(m_J + m_I)\nabla W(\mathbf{r}_J - \mathbf{r}_I, h)}{\|\mathbf{r}_J - \mathbf{r}_I\|^2}\right\} - \\ &-\frac{\Gamma^{-1}_{\beta\beta}}{n}\{[\langle \nabla_\alpha (m(\mathbf{r}_I)\mathbf{F}(\mathbf{r}_I))\rangle - \mathbf{F}(\mathbf{r}_I)\langle \nabla_\alpha m(\mathbf{r}_I)\rangle + m(\mathbf{r}_I)\langle \nabla_\alpha \mathbf{F}(\mathbf{r}_I)\rangle]\mathbf{N}^\alpha\}\end{aligned} \tag{3}$$

$$\mathbf{N}^{\alpha}\left(\mathbf{r}_I\right)=\left[\sum_{\Omega_{\mathbf{r}_I,h}} V_{\mathbf{r}_J}\nabla_{\alpha}W\left(\mathbf{r}_J-\mathbf{r}_I,h\right)\right] \tag{4}$$

$$\left\langle\nabla_{\alpha}\mathbf{F}\left(\mathbf{r}_I\right)\right\rangle=\sum_{\Omega_{\mathbf{r}_I,h}} V_{\mathbf{r}_J}\left[\mathbf{F}\left(\mathbf{r}_J\right)-\mathbf{F}\left(\mathbf{r}_I\right)\right]\nabla^{*}_{\alpha}W\left(\mathbf{r}_J-\mathbf{r}_I,h\right) \tag{5}$$

$$\nabla^{*}_{\alpha}W=\mathbf{A}^{-1}_{\alpha\beta}\nabla_{\beta}W,\ \ \mathbf{A}_{\alpha\beta}=\left[\sum_{\Omega_{\mathbf{r}_I,h}} V_{\mathbf{r}_J}\left[\mathbf{r}^{\alpha}_J-\mathbf{r}^{\alpha}_I\right]\nabla_{\beta}W\left(\mathbf{r}_J-\mathbf{r}_I,h\right)\right] \tag{6}$$

where $n=1,2,3$ is the spatial dimension, the gradient approximation $\left\langle\nabla_{\alpha}\mathbf{F}\left(\mathbf{r}_I\right)\right\rangle$ is computed using (5) and the tensor $\Gamma_{\alpha\beta}$ is defined by

$$\Gamma_{\alpha\beta}\left(\mathbf{r}_I\right)=\sum_{\Omega_{\mathbf{r}_I,h}} V_{\mathbf{r}_J}\frac{\left(\mathbf{r}^{\gamma}_J-\mathbf{r}^{\gamma}_I\right)\nabla_{\gamma}W\left(\mathbf{r}_J-\mathbf{r}_I,h\right)}{\left\|\mathbf{r}_J-\mathbf{r}_I\right\|^2}\left(\mathbf{r}^{\alpha}_J-\mathbf{r}^{\alpha}_I\right)\left(\mathbf{r}^{\beta}_J-\mathbf{r}^{\beta}_I\right) \tag{7}$$

Throughout this paper, the summation by repeated Greek indices is assumed. For multi-dimensional problems, the correction tensor $\Gamma_{\alpha\beta}\left(\mathbf{r}_I\right)$ is a matrix. If the particle $\mathbf{r}_I$ has entire stencil support (i.e., the domain support for all kernels $W\left(\mathbf{r}_J-\mathbf{r}_I,h\right)$ is entire and symmetric) then $\Gamma_{\alpha\beta}\left(\mathbf{r}_I\right)\approx\delta_{\alpha\beta}$, $\delta_{\alpha\beta}$ is the Kronecker symbol. Unfortunately, $\Gamma_{\alpha\beta}\left(\mathbf{r}_I\right)$ deviates from $\delta_{\alpha\beta}$ for the provided algorithm and, hence, it is important to minimize this deviation from $\delta_{\alpha\beta}$ in the new methods.

Remark 1 It is important to note that correction tensors $\Gamma_{\alpha\beta}$ and $\mathbf{A}_{\alpha\beta}$ are the same tensors. Indeed, using the following identity:

$$\begin{aligned}&\left[\mathbf{r}^{\alpha}_J-\mathbf{r}^{\alpha}_I\right]\frac{\left(\mathbf{r}^{\gamma}_J-\mathbf{r}^{\gamma}_I\right)\nabla_{\gamma}W\left(\mathbf{r}_J-\mathbf{r}_I,h\right)}{\left\|\mathbf{r}_J-\mathbf{r}_I\right\|^2}=\\&=\pm\frac{1}{h}\frac{dW}{dz}\frac{\left[\mathbf{r}^{\alpha}_J-\mathbf{r}^{\alpha}_I\right]}{\left\|\mathbf{r}_J-\mathbf{r}_I\right\|}=\nabla_{\alpha}W\left(\mathbf{r}_J-\mathbf{r}_I,h\right),\quad\forall\alpha\end{aligned} \tag{8}$$

where $z=\left\|\mathbf{r}_J-\mathbf{r}_I\right\|/h$, $\forall\mathbf{r}_J,\mathbf{r}_I\in\Omega\subset\mathbb{R}^n$, the following relations can be established:

$$\begin{aligned}&\Gamma_{\alpha\beta}\left(\mathbf{r}_I\right)=\sum_{\Omega_{\mathbf{r}_I,h}} V_{\mathbf{r}_J}\frac{\left(\mathbf{r}^{\gamma}_J-\mathbf{r}^{\gamma}_I\right)\nabla_{\gamma}W\left(\mathbf{r}_J-\mathbf{r}_I,h\right)}{\left\|\mathbf{r}_J-\mathbf{r}_I\right\|^2}\left(\mathbf{r}^{\alpha}_J-\mathbf{r}^{\alpha}_I\right)\left(\mathbf{r}^{\beta}_J-\mathbf{r}^{\beta}_I\right)=\\&=\sum_{\Omega_{\mathbf{r}_I,h}} V_{\mathbf{r}_J}\left[\mathbf{r}^{\alpha}_J-\mathbf{r}^{\alpha}_I\right]\nabla_{\beta}W\left(\mathbf{r}_J-\mathbf{r}_I,h\right)=\mathbf{A}_{\alpha\beta}\left(\mathbf{r}_I\right)\end{aligned} \tag{9}$$

To calculate coefficients in the scheme (3)–(7) is a trivial task. However, in general, it should be performed at each Newton-Raphson iteration in the non-linear case (i.e., $m=m\left(F\right)$). It also requires additional efforts to invert the correction matrix $\mathbf{A}_{\alpha\beta}$ (inversion of $n\times n$ matrices per each particle, where $n=1,2,3$ is the

spatial dimension) and storage cost of $\nabla_\alpha W(\mathbf{r}_J - \mathbf{r}_I, h)$, $\nabla^*_\alpha W(\mathbf{r}_J - \mathbf{r}_I, h)$, and corresponding $\Gamma^{-1}_{\alpha\alpha} = \mathbf{A}^{-1}_{\alpha\alpha}$ per each particle.

2.1 Kernel Property

A central point of the SPH formalism is the concept of the interpolating function (or kernel) through which the continuum properties of the medium are recovered from a discrete sample of N points with prescribed mass m_I (for conventional Lagrangian methods) or volume V_I (for fully Eulerian methods). In the Lagrangian description, these points move according to the specified governing laws, whereas these points are fixed in space for the Eulerian description. A good interpolating kernel must satisfy a few basic requirements: it must tend to the delta function in the continuum limit and has to be a continuous function with definite first derivatives at least. From a more practical point of view it is also advisable to deal with symmetric finite range kernels, the latter is to avoid N^2 calculations. In this paper, the cubic spline is used:

$$W(z,h) = \frac{\Xi}{h^n} \begin{cases} 1 - \frac{3}{2}z^2 + \frac{3}{4}z^3, & 0 \le z \le 1 \\ \frac{1}{4}(2-z)^3, & 1 \le z \le 2 \\ 0, & z > 2 \end{cases} \tag{10}$$

where $z = \left\| \mathbf{r}' - \mathbf{r} \right\| / h$, $\forall \mathbf{r}, \mathbf{r}' \in \Omega \subset \mathbb{R}^n$ and $\Xi = \frac{3}{2}, \frac{10}{7\pi}, \frac{1}{\pi}$ in 1D (i.e., $n = 1$), 2D (i.e., $n = 2$) and 3D (i.e., $n = 3$), respectively.

3 Meshless Transmissibilities

The well-known two-point flux approximation (TPFA) is a numerical scheme used in most commercial reservoir simulators for the pressure Eq. (1): $\mathbf{L}(p) = 0$. The net flow rate of a fluid (single phase and component fluid) from a cell I into neighbouring cells is obtained by summing fluxes over the neighbouring cells J:

$$\mathbf{q} = \sum_J \widetilde{T}_{JI} \left[p(\mathbf{r}_J) - p(\mathbf{r}_I) \right], \; T_{JI} \ge 0 \tag{11}$$

where $\widetilde{T}_{JI}$ is the transmissibility between cells J and I, $\mathbf{q}$ is the total flux through the boundary of the control volume located at the point $\mathbf{r}_I$. The transmissibility $\widetilde{T}_{JI}$

defined at an interior face f between cells J and I is calculated as

$$\widetilde{T}_{JI} = \frac{1}{\left[\frac{\left\|\mathbf{r}_{f,J}\right\|^2}{\mathbf{S}_f \mathbf{M} \mathbf{r}_{f,J}} + \frac{\left\|\mathbf{r}_{f,I}\right\|^2}{\mathbf{S}_f \mathbf{M} \mathbf{r}_{f,I}}\right]} \tag{12}$$

where $\mathbf{r}_{f,J}$ and $\mathbf{r}_{f,I}$ are the vectors from centres of cells J and I to the face f respectively, $\mathbf{S}_f$ is the area vector of the face f. In the case of $\mathbf{M}$-orthogonal mesh, when $\mathbf{M}\mathbf{S}_f$ and $[\mathbf{r}_J - \mathbf{r}_I]$ are collinear, the expression (11) reduces to the form of the central finite difference scheme and approximates the flux with $O\left(h^2\right)$ order of accuracy for any mobility tensor field $\mathbf{M}$. The expression (12) ensures that the flux into the adjoining region is continuous [8]. The TPFA scheme (11) is unconditionally monotone scheme. It is clear that the expression (3) cannot be written in the form (11) due to terms $\langle \nabla_\alpha \left(m\left(\mathbf{r}_I\right) \mathbf{F}\left(\mathbf{r}_I\right)\right)\rangle \mathbf{N}^\alpha$ and $\mathbf{F}\left(\mathbf{r}_I\right) \langle \nabla_\alpha m\left(\mathbf{r}_I\right)\rangle \mathbf{N}^\alpha$. Hence, it is only possible in this case to introduce a definition of a partial meshless transmissibility between particles $\mathbf{r}_J$ and $\mathbf{r}_I$ as follows:

$$T\left(\mathbf{r}_J, \mathbf{r}_I\right) = T_{JI} = \frac{\Gamma_{\beta\beta}^{-1}}{n} \times \left\{ \sum_{\Omega_{\mathbf{r}_I, h}} V_{\mathbf{r}_J} \frac{\left(\mathbf{r}_J - \mathbf{r}_I\right) \cdot \left(m_J + m_I\right) \cdot \nabla W\left(\mathbf{r}_J - \mathbf{r}_I, h\right)}{\left\|\mathbf{r}_J - \mathbf{r}_I\right\|^2} - V_{\mathbf{r}_J} m_I \nabla W\left(\mathbf{r}_J - \mathbf{r}_I, h\right) \mathbf{N}^\alpha \right\} \tag{13}$$

It is important to note that transmissibilities T_{JI} and $\widetilde{T}_{JI}$ have different physical units. Furthermore, it raises the question wherever the proposed scheme (3) is monotone. Hence, let Ω be a bounded domain in $\mathbb{R}^n$ (a compact) with a piecewise boundary $\partial\Omega = \bar{\Gamma}_D \cup \bar{\Gamma}_N$, $\bar{\Gamma}_D \cap \bar{\Gamma}_N = \emptyset$, where measure $\mu\left(\Gamma_D\right) \neq 0$, Γ_D is the part of the boundary corresponding to the Dirichlet boundary condition, Γ_N is the part of the boundary corresponding to the Neumann boundary condition. In the following sections this question will be analysed in details for some modified schemes by stating that the solution of the equation for $\mathbf{M}\left(\mathbf{r}, p\left(\mathbf{r}\right)\right) = m\left(\mathbf{r}, p\left(\mathbf{r}\right)\right) \cdot \mathbf{I}$, $m\left(\mathbf{r}, p\left(\mathbf{r}\right)\right) \geq 0$:

$$-\nabla\left(\mathbf{M}\left(\mathbf{r}, p\left(\mathbf{r}\right)\right) \nabla p\left(\mathbf{r}\right)\right) = g\left(\mathbf{r}\right), \ \forall \mathbf{r} \in \Omega \subset \mathbb{R}^n \tag{14}$$

is non-negative subject to its existence and that the solution p^k for each kth—Picard iteration is a non-negative vector and the linear system is solved exactly, $\mathbf{I}$ is the unit tensor. Modifications were introduced due to the following theorem.

Theorem 1 *The discretization scheme ((3)–(7)) is at least* $O\left(h^\omega\right)$, $1 \leq \omega < 2$ *order of accuracy in average for any scalar mobility field* $m\left(\mathbf{r}, p\left(\mathbf{r}\right)\right) \in C^2\left(\Omega\right) \geq 0$ *everywhere within the numerical domain* Ω *sufficiently far away from the boundary* $\partial\Omega$.

Proof Using Taylor series expansions about a point $\mathbf{r}_I$ and the relation (5), the following relations can be written:

$$\begin{aligned}\mathbf{F}(\mathbf{r}_J) = \mathbf{F}(\mathbf{r}_I) + \mathbf{F}_{,\alpha}(\mathbf{r}_I)\left[\mathbf{r}_J^\alpha - \mathbf{r}_I^\alpha\right] + \\ + \frac{1}{2}\mathbf{F}_{,\alpha\gamma}(\mathbf{r}_I)\left[\mathbf{r}_J^\alpha - \mathbf{r}_I^\alpha\right]\left[\mathbf{r}_J^\gamma - \mathbf{r}_I^\gamma\right] + O\left(h^3\right)\end{aligned} \tag{15}$$

$$m(\mathbf{r}_J) = m(\mathbf{r}_I) + m_{,\alpha}(\mathbf{r}_I)\left[\mathbf{r}_J^\alpha - \mathbf{r}_I^\alpha\right] + O\left(h^2\right) \tag{16}$$

$$m_I \langle \mathbf{F}(\mathbf{r}_I)\rangle_\alpha = m_I \mathbf{F}_{,\alpha}(\mathbf{r}_I) + O\left(h^2\right) \tag{17}$$

$$\sum_{\Omega_{\mathbf{r}_I,h}} V_{\mathbf{r}_J}\left[\mathbf{r}_J^\gamma - \mathbf{r}_I^\gamma\right]\nabla_\alpha^* W(\mathbf{r}_J - \mathbf{r}_I, h) = \delta_{\gamma\alpha}, \quad \forall\gamma,\alpha \tag{18}$$

$$\left[\mathbf{r}_J^\alpha - \mathbf{r}_I^\alpha\right]\frac{\left(\mathbf{r}_J^\gamma - \mathbf{r}_I^\gamma\right)\nabla_\gamma W(\mathbf{r}_J - \mathbf{r}_I, h)}{\|\mathbf{r}_J - \mathbf{r}_I\|^2} = \nabla_\alpha W(\mathbf{r}_J - \mathbf{r}_I, h), \quad \forall\alpha \tag{19}$$

Substituting relations ((15)–(17)) into the scheme (3) and taking into account the relations (18) and (19), it leads to the following relations:

$$\begin{aligned}&\sum_{\Omega_{\mathbf{r}_I,h}} V_{\mathbf{r}_J}\left[\mathbf{F}(\mathbf{r}_J) - \mathbf{F}(\mathbf{r}_I)\right]\frac{(\mathbf{r}_J - \mathbf{r}_I)\cdot(m_J + m_I)\cdot\nabla W(\mathbf{r}_J - \mathbf{r}_I, h)}{\|\mathbf{r}_J - \mathbf{r}_I\|^2} = \\ &= 2m(\mathbf{r}_I)\mathbf{F}_{,\alpha}(\mathbf{r}_I)\sum_{\Omega_{\mathbf{r}_I,h}} V_{\mathbf{r}_J}\left[\mathbf{r}_J^\alpha - \mathbf{r}_I^\alpha\right]\frac{(\mathbf{r}_J - \mathbf{r}_I)\cdot\nabla W(\mathbf{r}_J - \mathbf{r}_I, h)}{\|\mathbf{r}_J - \mathbf{r}_I\|^2} + \\ &+ m(\mathbf{r}_I)\mathbf{F}_{,\alpha\gamma}(\mathbf{r}_I)\sum_{\Omega_{\mathbf{r},h}} V_{\mathbf{r}_J}\left[\mathbf{r}_J^\alpha - \mathbf{r}_I^\alpha\right]\left[\mathbf{r}_J^\gamma - \mathbf{r}_I^\gamma\right]\frac{(\mathbf{r}_J - \mathbf{r}_I)\cdot\nabla W(\mathbf{r}_J - \mathbf{r}_I, h)}{\|\mathbf{r}_J - \mathbf{r}_I\|^2} \\ &+ m_{,\alpha}(\mathbf{r}_I)\mathbf{F}_{,\gamma}(\mathbf{r}_I)\sum_{\Omega_{\mathbf{r}_I,h}} V_{\mathbf{r}_J}\left[\mathbf{r}_J^\alpha - \mathbf{r}_I^\alpha\right]\left[\mathbf{r}_J^\gamma - \mathbf{r}_I^\gamma\right]\frac{(\mathbf{r}_J - \mathbf{r}_I)\cdot\nabla W(\mathbf{r}_J - \mathbf{r}_I, h)}{\|\mathbf{r}_J - \mathbf{r}_I\|^2} \\ &+ O\left(h^2\right)\end{aligned} \tag{20}$$

$$\begin{aligned}&\left[\langle\nabla_\alpha(m(\mathbf{r}_I)\mathbf{F}(\mathbf{r}_I))\rangle - \mathbf{F}(\mathbf{r}_I)\langle\nabla_\alpha m(\mathbf{r}_I)\rangle + m(\mathbf{r}_I)\langle\nabla_\alpha\mathbf{F}(\mathbf{r}_I)\rangle\right] = \\ &= 2m(\mathbf{r}_I)\mathbf{F}_{,\alpha}(\mathbf{r}_I) + O\left(h^2\right)\end{aligned} \tag{21}$$

The claim of the theorem can be seen from the comparison of relations (20) and (21) and the fact is that

$$\sum_{\Omega_{\mathbf{r}_I,h}} V_{\mathbf{r}_J}\left[\mathbf{r}_J^\alpha - \mathbf{r}_I^\alpha\right]\frac{\left(\mathbf{r}_J^\gamma - \mathbf{r}_I^\gamma\right)\nabla_\gamma W(\mathbf{r}_J - \mathbf{r}_I, h)}{\|\mathbf{r}_J - \mathbf{r}_I\|^2} = \mathbf{N}^\alpha, \ \forall\alpha \tag{22}$$

and

$$\frac{\Gamma_{\beta\beta}^{-1}}{n} \times \left(\sum_{\Omega_{\mathbf{r}_I,h}} V_{\mathbf{r}_J} \left[\mathbf{r}_J^{\gamma} - \mathbf{r}_I^{\gamma} \right] \left[\mathbf{r}_J^{\alpha} - \mathbf{r}_I^{\alpha} \right] \frac{\left(\mathbf{r}_J^{\beta} - \mathbf{r}_I^{\beta} \right) \nabla_{\beta} W \left(\mathbf{r}_J - \mathbf{r}_I, h \right)}{\left\| \mathbf{r}_J - \mathbf{r}_I \right\|^2} \right) = \\ = \delta_{\gamma\alpha} + O\left(h^{\omega} \right), \ 1 \leq \omega < 2, \ \forall \gamma, \alpha \tag{23}$$

for all points $\mathbf{r}_I$ located sufficiently far away from the boundary $\partial\Omega$. The order of accuracy $O\left(h^{\omega}\right)$ has to be understood in statistical average sense with some dispersion around the average value. The scheme ((3)–(7)) does not require exact expressions for the gradient (i.e., spatial derivatives) of the mobility field $\nabla_{\gamma} m\left(\mathbf{r}, p\right)$ to keep a higher order of accuracy for any mobility field. Hence, this scheme can be used with the a discontinuous (or piece-wise) mobility field $m\left(\mathbf{r}, p\left(\mathbf{r}\right)\right) \in L_2\left(\Omega\right)$. The case of a discontinuous mobility field is considered below.

4 Discontinuous Mobility Case

Using the same idea behind the expression (13) and heterogeneous discontinues mobility field $m\left(\mathbf{r}\right)$, it can be shown that the effect of requiring the flux into the adjoining region to be continuous leads to the equivalent to the expression (13) in terms of the effective mobility between particle $\mathbf{r}_I$ and $\mathbf{r}_J$ (clearly and Monaghan [8]):

$$m^{eff} = \left(\frac{m\left(\mathbf{r}_J\right) \cdot m\left(\mathbf{r}_I\right)}{m\left(\mathbf{r}_J\right) + m\left(\mathbf{r}_I\right)} \right) \tag{24}$$

It can be seen that the effective mobility $\left(m\left(\mathbf{r}_J\right) + m\left(\mathbf{r}_I\right)\right)$ does not guarantee the continuity of the flux between the particles with discontinuous mobilities. Taking this into account and applying the relation (24), the final discretization scheme for the discontinuous scalar mobility field can be written as

$$\left\langle \nabla_{\alpha} \left(m\left(\mathbf{r}_I\right) \nabla_{\alpha} \mathbf{F}\left(\mathbf{r}_I\right) \right) \right\rangle = \\ \frac{4 \cdot \Gamma_{\beta\beta}^{-1}}{n} \left\{ \sum_{\Omega_{\mathbf{r}_I,h}} V_{\mathbf{r}_J} \cdot m^{eff} \cdot \left[\mathbf{F}\left(\mathbf{r}_J\right) - \mathbf{F}\left(\mathbf{r}_I\right) \right] \frac{\left(\mathbf{r}_J^{\alpha} - \mathbf{r}_I^{\alpha} \right) \cdot \nabla_{\alpha} W\left(\mathbf{r}_J - \mathbf{r}_I, h\right)}{\left\| \mathbf{r}_J - \mathbf{r}_I \right\|^2} \right\} \\ - \frac{2 \cdot \Gamma_{\beta\beta}^{-1}}{n} \left\{ \left(\sum_{\Omega_{\mathbf{r}_I,h}} V_{\mathbf{r}_J} \cdot m_I \cdot \left[\mathbf{F}\left(\mathbf{r}_J\right) - \mathbf{F}\left(\mathbf{r}_I\right) \right] \nabla_{\alpha}^{*} W\left(\mathbf{r}_J - \mathbf{r}_I, h\right) \right) \mathbf{N}^{\alpha} \right\} \tag{25}$$

This numerical scheme is the final one for the heterogeneous discontinuous isotropic scalar mobility field, which is used for numerical tests throughout this paper. It ensures that the flux is automatically continuous between particles with the reasonable accuracy. Multiple regions with substantially different fluid properties and specific mobilities can then be simulated.

The analytical analysis of the aforementioned scheme for a fully anisotropic mobility tensor field is complicated. However, the numerical analysis reveals that these schemes do not produce a reasonable approximation for a linear pressure field for the anisotropic mobility tensor field. The following section describes a scheme applicable to a fully anisotropic mobility tensor field.

4.1 Anisotropic Case

Generally speaking, any second order tensor can be decomposed into the spherical and deviatorical parts. In the case of continuum mechanics, the decomposition of the second order tensor (e.g., stress tensor or strain tensor) into their volumetric and deviatoric components have certain physical justifications. This step is done in order to distinguish between volumetric and shear responses. Hence, any mobility field $\mathbf{M}(\mathbf{r}, p(\mathbf{r}))$ can also be split as:

$$\mathbf{M}(\mathbf{r}, p(\mathbf{r})) = M^S(\mathbf{r}, p(\mathbf{r})) \cdot \mathbf{I} + \mathbf{M}^D(\mathbf{r}, p(\mathbf{r})), \; M^S(\mathbf{r}, p(\mathbf{r})) = \frac{1}{3} tr(\mathbf{M}(\mathbf{r})) \tag{26}$$

where $M^S(\mathbf{r}, p(\mathbf{r})) \cdot \mathbf{I}$ is the spherical part of the mobility tensor, $\mathbf{M}^D(\mathbf{r}, p(\mathbf{r}))$ is the deviatoric part of the mobility tensor. In addition, the Darcy velocity can be written as

$$\begin{aligned} &\mathbf{v}(\mathbf{r}) = \mathbf{v}^S(\mathbf{r}) + \mathbf{v}^D(\mathbf{r}), \\ &\mathbf{v}^S(\mathbf{r}) = -M^S(\mathbf{r}, p(\mathbf{r})) \nabla p(\mathbf{r}), \\ &\mathbf{v}^D(\mathbf{r}) = -\mathbf{M}^D(\mathbf{r}, p(\mathbf{r})) \nabla p(\mathbf{r}) \end{aligned} \tag{27}$$

where $\mathbf{v}^S(\mathbf{r})$ is the volumetric velocity, $\mathbf{v}^D(\mathbf{r})$ is the deviatoric velocity. The problem discussed in this paper is the discretization of the elliptic operator:

$$\nabla \mathbf{v}(\mathbf{r}) = \nabla \mathbf{v}^S(\mathbf{r}) + \nabla \mathbf{v}^D(\mathbf{r}) = g(\mathbf{r}), \; \forall \mathbf{r} \in \Omega \subset \mathbb{R}^n \tag{28}$$

Hence, the discretization scheme can be constructed in two steps. The first step is to discretize the volumetric term $\nabla \mathbf{v}^S(\mathbf{r})$ following the scheme (25):

$$\begin{aligned} &-\langle \nabla \mathbf{v}^S(\mathbf{r}) \rangle = \\ &\frac{4 \cdot \Gamma_{\beta\beta}^{-1}}{n} \left\{ \sum_{\Omega_{\mathbf{r}_I, h}} V_{\mathbf{r}_J} \cdot M_{eff}^S \cdot [\mathbf{F}(\mathbf{r}_J) - \mathbf{F}(\mathbf{r}_I)] \frac{\left(\mathbf{r}_J^\alpha - \mathbf{r}_I^\alpha\right) \cdot \nabla_\alpha W(\mathbf{r}_J - \mathbf{r}_I, h)}{\|\mathbf{r}_J - \mathbf{r}_I\|^2} \right\} \\ &-\frac{2 \cdot \Gamma_{\beta\beta}^{-1}}{n} \left\{ \left(\sum_{\Omega_{\mathbf{r}_I, h}} V_{\mathbf{r}_J} \cdot M^S(\mathbf{r}_I) \cdot [\mathbf{F}(\mathbf{r}_J) - \mathbf{F}(\mathbf{r}_I)] \nabla_\alpha^* W(\mathbf{r}_J - \mathbf{r}_I, h) \right) \mathbf{N}^\alpha \right\} \end{aligned} \tag{29}$$

where M^S_{eff} is defined as

$$M^S_{eff} = \left(\frac{M^S(\mathbf{r}_J) \cdot M^S(\mathbf{r}_I)}{M^S(\mathbf{r}_J) + M^S(\mathbf{r}_I)} \right) \tag{30}$$

The second step is to discretize the deviatoric term $\nabla \mathbf{v}^D(\mathbf{r})$ as follows:

$$\langle \nabla \mathbf{v}^D(\mathbf{r}) \rangle = \sum_{\Omega_{\mathbf{r}_I,h}} V_{\mathbf{r}_J} \left[\langle \mathbf{v}^D(\mathbf{r}_J) \rangle - \langle \mathbf{v}^D(\mathbf{r}_I) \rangle \right] \nabla^* W(\mathbf{r}_J - \mathbf{r}_I, h) \tag{31}$$

$$\begin{aligned} \langle \mathbf{v}^D(\mathbf{r}_I) \rangle &= -\mathbf{M}^D \langle \nabla p(\mathbf{r}_I) \rangle, \\ \langle \nabla p(\mathbf{r}_I) \rangle &= \sum_{\Omega_{\mathbf{r}_I,h}} V_{\mathbf{r}_J} \left[p(\mathbf{r}_J) - p(\mathbf{r}_I) \right] \nabla^* W(\mathbf{r}_J - \mathbf{r}_I, h) \end{aligned} \tag{32}$$

The numerical scheme (31)–(32) can be directly applied to discretize the original Laplace operator (1) with the anisotropic mobility tensor $\mathbf{M}(\mathbf{r}, p(\mathbf{r})) \in L_2(\Omega)$. This scheme provides an exact answer for the linear pressure distribution in both homogeneous and heterogeneous (linear) mobility fields. Figure 1 shows the comparison between numerical and analytical values of the generalized Laplace operator for the linear pressure distribution $p(\mathbf{r}) = 11 \cdot x + 5 \cdot y + 17$ and for mobility tensors defined as

$$\begin{aligned} (a) \quad \mathbf{M}(\mathbf{r}) &= \begin{pmatrix} 6 & 3 \\ 3 & 5 \end{pmatrix}, \\ (b) \quad \mathbf{M}(\mathbf{r}) &= \begin{pmatrix} 10 + 10 \cdot x + 6 \cdot y & 2 + 2 \cdot x + 2 \cdot y \\ 2 + 2 \cdot x + 2 \cdot y & 4 + 4 \cdot x + y \end{pmatrix} \end{aligned} \tag{33}$$

The observed error is of a machine tolerance, which confirms theoretical claims by numerical experiments. Incompleteness of the kernel support combined with the

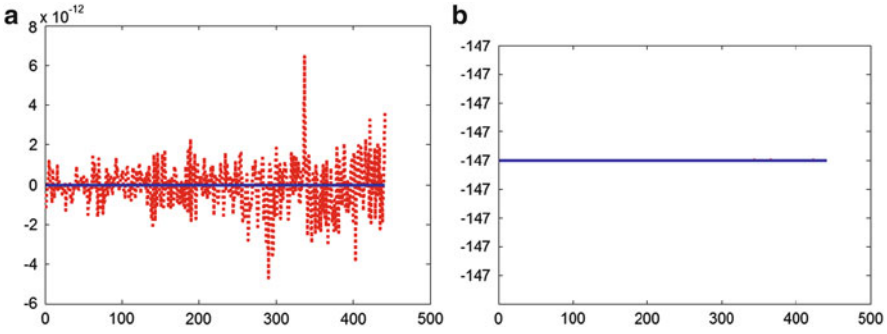

Fig. 1 Comparison between analytical and numerical values for the generalized Laplace operator for the linear pressure and (a) homogenous mobility field, and (b) heterogeneous mobility field defined in (33)

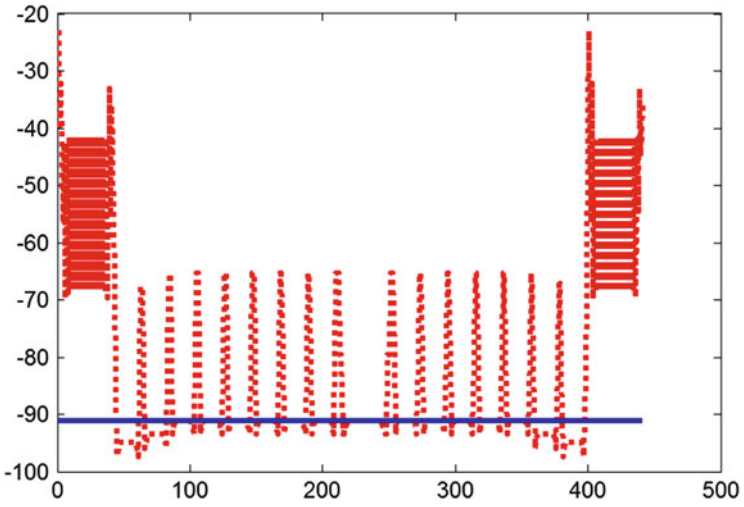

Fig. 2 Comparison between analytical and numerical values for the generalized Laplace operator for the quadratic pressure and homogenous mobility field defined in (33) case (a)

lack of consistency of the kernel interpolation in conventional meshless method results in fuzzy boundaries. For the scheme (31)–(32), the error starts occurring at the boundary particles for quadratic and higher polynomials of the pressure distribution. Figure 2 demonstrates the values of the generalized Laplace operator for the homogeneous mobility field in (33) case (a) for the quadratic pressure distribution $p(\mathbf{r}) = \frac{1}{2}\left(11 \cdot x^2 + 5 \cdot y^2 + 17\right)$. In spite of perfectly adequate general discretization properties, the numerical scheme (31)–(32) is not unconditionally monotone. Knowledge of the capabilities and limitations of these different numerical schemes leads to a better understanding of their impact on various applications and future research on improving and extending modeling capabilities. Hence, it is important to make here a few remarks.

Remark 2 The aforementioned schemes (25) and (31)–(32) can be written in the form:

$$\langle \mathbf{L}(p(\mathbf{r})) \rangle = \sum_S \bar{T}_{SI}^M p_S, \ \sum_S \bar{T}_{SI}^M = 0 \tag{34}$$

where operator $\mathbf{L}$ is defined by either M^S or $\mathbf{M}^D$ and $\bar{T}_{SI}^M$ is the meshless transmissibilities. In the case of the conventional Laplace operator $\nabla^2 p$ (i.e., $m(\mathbf{r}_I) \equiv 1$), it

can be derived $\forall \mathbf{r}_I$:

$$\begin{aligned} &(a) \sum_S \bar{T}_{SI}^M = 0, \\ &(b) \sum_S \bar{T}_{SI}^M \left[\mathbf{r}_S - \mathbf{r}_I\right] = \mathbf{0}, \\ &(c) \frac{1}{2} \sum_S \bar{T}_{SI}^M \left[\mathbf{r}_S - \mathbf{r}_I\right] \cdot \left[\mathbf{r}_S - \mathbf{r}_I\right]^T \neq \mathbf{I} \end{aligned} \tag{35}$$

This follows from the fact that the Taylor expansion of the pressure around the point $\mathbf{r}_I$ can be written as

$$\begin{aligned} p\left(\mathbf{r}_S\right) = p\left(\mathbf{r}_I\right) + \nabla p\left(\mathbf{r}_I\right) \cdot \left[\mathbf{r}_S - \mathbf{r}_I\right] + \\ + \frac{1}{2} \left[\mathbf{r}_S - \mathbf{r}_I\right]^T \cdot \nabla \otimes \nabla p\left(\mathbf{r}_I\right) \cdot \left[\mathbf{r}_S - \mathbf{r}_I\right] + O\left(h^3\right) \end{aligned} \tag{36}$$

The constraints (35) lead to significant differences between proposed meshless multi-point flux approximation schemes and meshfree finite difference approximation schemes (see, Seibold [32]). It is important to recall here that meshfree finite difference approximation schemes, which satisfy the constraints (a)–(b) and

$$\frac{1}{2} \sum_S \bar{T}_{SI}^M \left[\mathbf{r}_S - \mathbf{r}_I\right] \cdot \left[\mathbf{r}_S - \mathbf{r}_I\right]^T = \mathbf{I}$$

are based on the following steps: (1) to define the neighbours list for each point (it is important to choose more neighbours than constraints); (2) to select unique stencil which can be satisfied addition requirements (e.g., monotonicity Seibold [32]).

Remark 3 The scheme (31)–(32) can be applied directly to the Darcy velocity (27) with the full mobility tensor. Furthermore, the following theorem is valid for the full mobility tensor:

Theorem 2 *The discretization scheme (31)–(32) is at least of* $O\left(h^2\right)$ *order of accuracy for any differentiable heterogeneous full mobility tensor field everywhere within the numerical domain* Ω.

The proof of *Theorem* 2 can be seen from the construction of the scheme (31)–(32). However, the scheme (31)–(32) is not unconditionally monotone but as was shown by Seibold [32] in case of meshfree finite difference methods, it is possible to have positive stencils in the scheme (31)–(32), i.e. all neighbor entries are of the same sign.

Remark 4 The schemes (25) and (31)–(32) do not require exact expressions for the gradient (i.e., spatial derivatives) of the mobility field $\nabla_\gamma \mathbf{M}_{\alpha\beta}\left(\mathbf{r}, p\left(\mathbf{r}\right)\right) = \mathbf{M}_{\alpha\beta,\gamma}\left(\mathbf{r}, p\left(\mathbf{r}\right)\right)$ to keep $O(h^\alpha)$, $1 \leq \alpha < 2$ order of accuracy) for any mobility field $\mathbf{M}\left(\mathbf{r}, p\left(\mathbf{r}\right)\right) \in L_2\left(\Omega\right)$. Hence, an important feature of reservoir simulations

that the mobility field $\mathbf{M}(\mathbf{r}, p(\mathbf{r}))$ is to be a discontinuous (or piece-wise function) is allowed in this scheme.

Remark 5 Applying aforementioned meshless discretization schemes to the elliptic problem $\mathbf{L}(p) = 0$ results in formulating a general non-linear system which can be solved by iterative Newton-Raphson or Picard methods leading to the sequence of linear systems with the matrix $\mathbf{A} = \left(a_{ij}\right)_{1 \le i \le n, 1 \le j \le n} \in \mathbb{R}^{n \times n}$:

$$\mathbf{A}p = b \tag{37}$$

where the pressure vector p contains approximations to the pressure $p(\mathbf{r})$. It is assumed that $\mathbf{L}(p(\mathbf{r})) = 0$ admits a unique solution with a discontinuity permeability tensor. The I-th row of the matrix $\mathbf{A}$ consists of the stencil corresponding to the point $\mathbf{r}_I$. Let the unknowns be labeled by an index set N same as particles labels. We consider square matrices $\mathbf{A} \in \mathbb{R}^{n \times n}$.

Definition 1 A matrix $\mathbf{A}$ is called essentially irreducible if every point is connected to a Dirichlet boundary point.

The matrix $\mathbf{A}$ resulting from the meshless discretization is a essentially irreducible, which is guaranteed by selecting Kernel supports and the *Heine-Borel theorem*.

Remark 6 Meshless multi-point flux approximation matrices are in general non-symmetric. Consider two points $\mathbf{r}_I$ and $\mathbf{r}_J$ with the corresponding smoothing lengths h_I and h_J. Since each stencil entry depends on the smoothing length, the point $\mathbf{r}_J$ influences the matrix entry a_{ij} if $\|\mathbf{r}_J - \mathbf{r}_I\| \le \lambda \cdot h_I$ whereas $\mathbf{r}_I$ does not influence the matrix entry a_{ji} if $\|\mathbf{r}_J - \mathbf{r}_I\| > \lambda \cdot h_J$, where λ is the scaling factor defined by the shape of the Kernel function. A number of symmetrization methods can be used to overcome this problem. In this paper, the homogeneous smoothing length $h_I = h_J,\ \forall I, J$ is used.

This ends the derivation of a meshless multi-point flux approximation method that can be used to solve different boundary value problems.

5 Numerical Experiments

The verification process is intended to provide, and quantify, the confidence in numerical modelling and the results from the corresponding simulations. Therefore, in order to be confident that the proposed meshless multi-point flux approximation provides the announced accuracy of the elliptic operator (1), it was tested for several functions and different media (diagonal and non-diagonal mobility tensors).

In this section, the results of the numerical experiments using the proposed scheme in Sect. 2.1 are presented, which confirm some of the theoretical results from the previous sections. The problems are solved using 2D (i.e., $n = 2$) square domains (see Fig. 3) with Dirichlet boundary conditions. Following the work by

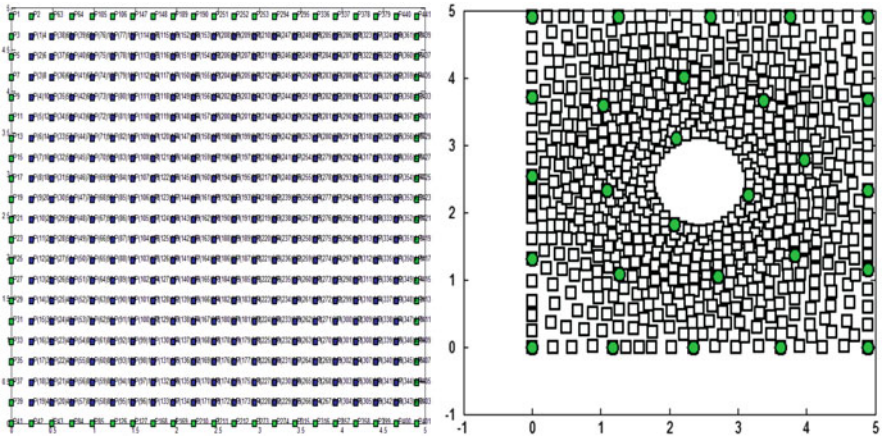

Fig. 3 Numerical domains with different particle distributions

Lukyanov [24–26], the inhomogeneous Dirichlet test cases are considered for the verification purpose in this paper subject to the assumption that $g(\mathbf{r}) = 0,\ \forall \mathbf{r} \in \Omega \subset \mathbb{R}^2$, linear and quadratic pressure boundary conditions:

$$\begin{aligned} p(\mathbf{r}) &= 10 \cdot x + 12 \cdot y + 1, \forall \mathbf{r} = (x, y) \in \partial\Omega \subset \mathbb{R}^2, \\ p(\mathbf{r}) &= \frac{1}{2} \cdot \left(11 \cdot x^2 + 12 \cdot y^2 + 1\right), \forall \mathbf{r} = (x, y) \in \partial\Omega \subset \mathbb{R}^2 \end{aligned} \tag{38}$$

The rectangular 2D (i.e., $n = 2$) domain $\Omega = \{(x, y) \in [0; L] \times [0; H]\} \subset \mathbb{R}^n$ of width $L = 4.9$ m and height $H = 4.9$ m with and without a circle inclusion are considered (see, Fig. 3 cases (a) and (b), respectively).

The components of the heterogeneous mobility field in SI units are defined using the normal distribution with the mean mobility tensor $\mathbf{M}(\mathbf{r})$ and standard deviation matrix $\mathbf{D}(\mathbf{r})$:

$$\mathbf{M}(\mathbf{r}) = \begin{pmatrix} 12 & 5 \\ 5 & 12 \end{pmatrix}, \quad \mathbf{D}(\mathbf{r}) = \begin{pmatrix} 0.1 & 0.2 \\ 0.2 & 0.1 \end{pmatrix} \tag{39}$$

It is clear that the pressure field depicted at Figs. 4 and 5 does not have any spurious oscillations and, hence, satisfies a discrete maximum principle. This suggests that the meshless multi-point flux approximation provides a good approximation of the pressure gradient in the flux computation at least for this study.

Convergence rates are established by running for five levels of particles refinement, starting with the particle distance $h = 0.245$ m on level 1 and refining by a factor of 2 for each successive level. Assuming that the error takes the form $C_p h^{\alpha_p}$, where C_p and α_p are determined to give the best least square fit the data. We consider two types of particle distributions: (a) uniform particle distribution and

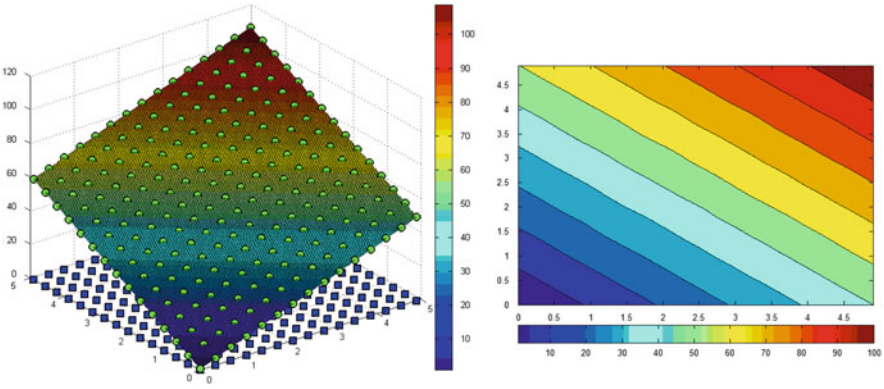

Fig. 4 Single-phase incompressible problem with full-permeability tensor (Cartesian grid)

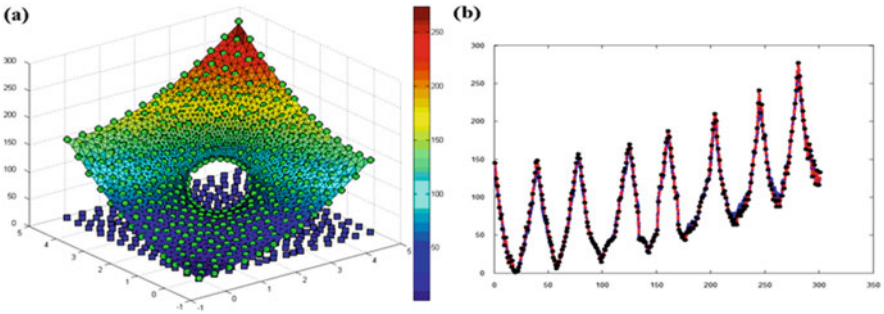

Fig. 5 Different approximate solutions of Dirichlet boundary value problems with the Laplace operator (1) and nonlinear boundary conditions: (**a**) boundary and internal pressure distribution, (**b**) comparison of solutions for different particle distributions

(b) non-uniform particle distribution that is a random perturbation of the uniform particles. The results for the Dirichlet problems using the numerical domain Fig. 3 cases (a) are presented in Table 1. Quadrature rules are used for calculating the error:

$$\|p - p_h\|^2 = \sum_{\xi_K} V_{\xi_K} \left(p\left(\xi_K\right) - p_h\left(\xi_K\right)\right)^2 \tag{40}$$

that is, the results presented for the pressure. The approximation rate for the pressure is between $O\left(h\right)$ and $O\left(h^2\right)$. Although, there is no solid proof that the proposed scheme is unconditionally monotone. Numerical results indicate that a relatively small spacing between particles leads to the unconditional monotonicity condition.

Table 1 Approximation rates for the relatively simple Dirichlet problem $\|p - p_h\| \leq C_p h^{\alpha_p}$

Tensor	Particle distribution	C_p	α_p
Diagonal	Uniform	0.348	1.991
Diagonal	Weakly distorted	0.231	1.923
Diagonal	Highly distorted	0.257	1.732
Non-diagonal	Uniform	0.391	1.990
Non-diagonal	Weakly distorted	0.272	1.919
Non-diagonal	Highly distorted	0.293	1.727

6 Conclusion

Several methods have been proposed to address the difficulties involved in calculating second-order derivatives with SPH for heterogeneous scalar mobility fields by calculating the Hessian or requiring that the discrete equations exactly reproduce quadratic or higher order polynomials. In this paper, the proposed method provides a simple discretization of the generalized Laplace operator occurring in modeling fluid flows in anisotropic porous media, anisotropic viscous fluids.

The resulting meshless multi-point flux scheme not only ensures first order consistency $O(h)$ but also improves the particle deficiency (kernel support incompleteness) problem. The proposed scheme was tested by solving an inhomogeneous Dirichlet boundary value problem for the generalized Laplacian equation with good accuracy. Furthermore, including gradient corrections significantly improves the Laplacian approximation near boundaries, although this requires an $n \times n$ matrix inversion for each particle.

The discretization was tested for several boundary value problems using a variety of boundary conditions. Approximation rates of the discretization scheme is smaller with particle disorder; however, the solution remains robust. It is possible that these rates may be improved with different approximations of the spherical part of the Darcy velocity.

References

1. I. Aavatsmark, An introduction to multipoint flux approximations for quadrilateral grids. Comput. Geosci. **6**, 405–432 (2002)
2. I. Aavatsmark, T. Barkve, O. Bøe, T. Mannseth, Discretization on unstructured grids for inhomogeneous, anisotropic media. Part I: derivation of the methods. Part II: discussion and numerical results. SIAM J. Sci. Comput. **19**, 1700–1716 (1998)
3. I. Aavatsmark, T. Barkve, T. Mannseth, Control-volume discretization methods for 3d quadrilateral grids in inhomogeneous, anisotropic reservoirs. SPE J. **3**, 146–154 (1998)
4. J. Bonet, S. Kulasegaram, Correction and stabilization of smooth particle hydrodynamics methods with applications in metal forming simulations. Int. J. Numer. Methods Eng. **47**, 1189–1214 (2000)
5. J. Bonet, T.S.L. Lok, Variational and momentum preservation aspects of smooth particle hydrodynamic formulations. Comput. Methods Appl. Mech. Eng. **180**, 97–115 (1999)

6. L. Brookshaw, A method of calculating radiative heat diffusion in particle simulations. Proc. Astron. Soc. Aust. **6**, 207–210 (1985)
7. J.K. Chen, J.E. Beraun, C.J. Jih, Completeness of corrective smoothed particle method for linear elastodynamics. Comput. Mech. **24**, 273–285 (1999)
8. P.W. Cleary, J.J. Monaghan, Conduction modelling using smoothed particle hydrodynamics. J. Comput. Phys. **148**, 227–264 (1999)
9. F. Colin, R. Egli, F.Y. Lin, Computing a null divergence velocity field using smoothed particle hydrodynamics. J. Comput. Phys. **217**, 680–692 (2006)
10. S.J. Cummins, M. Rudman, An SPH projection method. J. Comput. Phys. **152**, 584–607 (1999)
11. M.G. Edwards, Unstructured, control-volume distributed, full-tensor finite volume schemes with flow based grids. Comput. Geosci. **6**, 433–452 (2002)
12. M.G. Edwards, C.F. Rogers, Finite volume discretization with imposed flux continuity for the general tensor pressure equation. Comput. Geosci. **2**, 259–290 (1998)
13. J. Fang, A. Parriaux, A regularized lagrangian finite point method for the simulation of incompressible viscous flows. J. Comput. Phys. **227**, 8894–8908 (2008)
14. D.A. Fulk, D.W. Quinn, An analysis of 1-d smoothed particle hydrodynamics kernels. J. Comput. Phys. **126**, 165–180 (1996)
15. X.Y. Hu, N.A. Adams, A multi-phase SPH method for macroscopic and mesoscopic flows. J. Comput. Phys. **213**, 844–861 (2006)
16. M. Jubelgas, V. Springel, K. Dolag, Thermal conduction in cosmological SPH simulations. Mon. Not. R.. Astron. Soc. **351**, 423–435 (2004)
17. R.A. Klausen, T.F. Russell, Relationships among some locally conservative discretization methods which handle discontinuous coefficients. Comput. Geosci. **8**, 341–377 (2004)
18. S.H. Lee, L.J. Durlofsky, M.F. Lough, W.H. Chen, Finite difference simulation of geologically complex reservoirs with tensor permeabilities. SPE Reservoir Eval. Eng. **1**, 567–574 (1998)
19. S.H. Lee, P. Jenny, H.A. Tchelepi, A finite-volume method with hexahedral multiblock grids for modeling flow in porous media. Comput. Geosci. **6**, 353–379 (2002)
20. E.-S. Lee, C. Moulinec, R. Xu, D. Violeau, D. Laurence, P. Stansby, Comparison of weakly compressible and truly incompressible algorithms for the SPH mesh free particle method. J. Comput. Phys. **227**, 8417–8436 (2008)
21. W.K. Liu, S. Jun, Multiple-scale reproducing kernel particle method for large deformation problems. Int. J. Numer. Methods Eng. **41**, 1339–1362 (1998)
22. G.R. Liu, M.B. Liu, *Particle Hydrodynamics: A Meshfree Particle Method* (World Scientific Publishing, Singapore, 2003), 449 p.
23. A.A. Lukyanov, Numerical modelling of the material failure under shock loading using particle method, Izvetiya Tula State University. Estestvennonauchn. Ser. **1**, 54–65 (2007)
24. A.A. Lukyanov, Meshless upscaling method and its application to a fluid flow in porous media, in *ECMOR XII Conference Proceedings (2010)*, Oxford (2010)
25. A.A. Lukyanov, Meshless multi-point flux approximation of fluid flow in porous media, in *SPE Reservoir Simulation Symposium (2011), SPE* (2011), 141617 pp.
26. A.A. Lukyanov, Adaptive fully implicit multi-scale meshless multi-point flux method for fluid flow in heterogeneous porous media, in *ECMOR XIII Conference Proceedings (2012)*, Biarritz (2012)
27. A.A. Lukyanov, V.B. Pen'kov, Numerical simulation of solids deformation by a meshless method. Vestn. Samar. Gos. Univ. Estestvennonauchn. Ser. **6**, 62–70 (2007)
28. M.J. Mlacnik, L.J. Durlofsky, Unstructured grid optimization for improved monotonicity of discrete solutions of elliptic equations with highly anisotropic coefficients. J. Comput. Phys. **216**, 337–361 (2006)
29. J.P. Morris, P.J. Fox, Y. Zhu, Modeling low Reynolds number incompressible flows using SPH. J. Comput. Phys. **136**, 214–226 (1997)
30. P. Randles, L. Libersky, Smoothed particle hydrodynamics: some recent improvements and applications. Comput. Methods Appl. Mech. Eng. **139**, 375–408 (1996)
31. H.F. Schwaiger, An implicit corrected SPH formulation for thermal diffusion with linear free surface boundary conditions. Int. J. Numer. Methods Eng. **75**, 647–671 (2008)

32. B. Seibold, M-matrices in meshless finite difference methods, Dissertation, Department of Mathematics, University of Kaiserslautern, 2006
33. S. Shao, E.Y.M. Lo, Incompressible SPH method for simulating newtonian and non-newtonian flows with a free surface. Adv. Water Resour. **26**, 787–800 (2003)
34. S. Zhang, S. Kuwabara, T. Suzuki, Y. Kawano, K. Morita, K. Fukuda, Simulation of solid-fluid mixture flow using moving particle methods. J. Comput. Phys. **228**, 2552–2565 (2009)